Molecular Therapy
Nucleic Acids
Original Article

Proof-of-concept study for liver-directed miQURE technology in a dyslipidemic mouse model

Vanessa Zancanella,[1] Astrid Vallès,[1] Jolanda M.P. Liefhebber,[1] Lieke Paerels,[1] Carlos Vendrell Tornero,[1] Hendrina Wattimury,[1] Tom van der Zon,[1] Kristel van Rooijen,[1] Monika Golinska,[1] Tamar Grevelink,[1] Erich Ehlert,[1] Elsbet Jantine Pieterman,[2] Nanda Keijzer,[2] Hans Marinus Gerardus Princen,[2] Geurt Stokman,[2] and Ying Poi Liu[1]

[1]uniQure biopharma B.V., Department of Research and Development, 1105 BP, Amsterdam, The Netherlands; [2]TNO Metabolic Health Research, Sylviusweg 71 2333 BE Leiden, The Netherlands

A gene-silencing platform (miQURE) has been developed and successfully used to deliver therapeutic microRNA (miRNA) to the brain, reducing levels of neurodegenerative disease-causing proteins/RNAs via RNA interference and improving the disease phenotype in animal models. This study evaluates the use of miQURE technology to deliver therapeutic miRNA for liver-specific indications. Angiopoietin-like 3 (*ANGPTL3*) was selected as the target mRNA because it is produced in the liver and because loss-of-function *ANGPTL3* mutations and/or pharmacological inhibition of ANGPTL3 protein lowers lipid levels and reduces cardiovascular risk. Overall, 14 candidate *miRNA* constructs were tested *in vitro*, the most potent of which (*miAngE*) was further evaluated in mice. rAAV5-*miAngE* led to dose-dependent ($\leq -77\%$) decreases in *Angptl3* mRNA in WT mice with $\leq -90\%$ reductions in plasma ANGPTL3 protein. In dyslipidemic APOE*3-Leiden.CETP mice, AAV5-*miAngE* significantly reduced cholesterol and triglyceride levels vs. vehicle and scrambled (*miSCR*) controls when administrated alone, with greater reductions when co-administered with lipid-lowering therapy (atorvastatin). A significant decrease in total atherosclerotic lesion area (-58% vs. *miSCR*) was observed in AAV5-*miAngE*-treated dyslipidemic mice, which corresponded with the maintenance of a non-diseased plaque phenotype and reduced lesion severity. These results support the development of this technology for liver-directed indications.

INTRODUCTION

RNA interference (RNAi) is an evolutionary conserved and sequence-specific gene-silencing mechanism in eukaryotes[1,2] triggered by small RNA classes, e.g., microRNAs (miRNAs), endogenous small interfering RNAs, and PIWI-associated RNAs (piRNAs, which silence transposable elements). miRNAs play a key role in regulating cellular gene expression at a posttranscriptional level. More than a thousand human miRNAs have been identified, which regulate the expression of ~30% of all known genes.[3] Given their abundance and importance, there is a significant drive to discover endogenous miRNAs and harness their gene-silencing capabilities. Engineered miRNA mimics have, therefore, also been widely explored for therapeutic purposes.[4–11] miQURE technology comprises a gene cassette expressing an miRNA of interest within the miR-451 scaffold, which targets a complementary mRNA.[12] The cassette is delivered to target cells using a recombinant AAV5 (rAAV5) vector, and the genetic payload is released directly into the nucleus, where it remains primarily episomal. The episome expresses the miRNA as a pri-miRNA precursor that folds into a hairpin scaffold comprising a double-stranded stem and a single-stranded loop.[13] In the majority of miRNA scaffolds, the loop is cleaved by Dicer, yielding a mature miRNA containing the "guide" strand (the therapeutic sequence) and its complementary "passenger" strand. The passenger strand is usually degraded or loaded into RISC at a low frequency leading to the repression of off-target genes. The miQURE platform uses am miR-451 scaffold, which undergoes non-canonical Dicer-independent processing (via Argonaute-2 [Ago2]).[14,15] The miR-451 scaffold, therefore, produces miRNA without a complementary passenger strand, significantly reducing the rate of off-target effects[16] and the dysregulation of endogenous gene expression that may be associated with the production of engineered miRNAs.[13–15,17–20] miQURE technology is currently used to deliver investigational gene therapies for the treatment of Huntington's disease (HD),[12] a neurodegenerative disorder caused by an accumulation of toxic huntingtin (HTT) protein in the brain. In HD animal models, a single intrastriatal infusion of rAAV5-*miHtt* resulted in dose-dependent increases in *miHTT* levels in the deep brain structures associated with HD pathology with subsequent decreases in *Htt* mRNA and no evidence of off-target effects.[21–25] Levels of transgene expression correlated with vector DNA copy numbers (VCNs) from the same brain region, and reductions in *Htt* mRNA were accompanied by HTT protein reductions lasting at least 12 months in HD mice[21] and minipigs.[23] In HD mice, significant reductions in HTT aggregates were associated with reversed neuron dysfunction prior to neuron death, improved HD symptoms, and extended survival.[21] The product received Fast Track Designation from the Food and Drug Administration in 2019,

Received 16 September 2022; accepted 4 April 2023;
https://doi.org/10.1016/j.omtn.2023.04.004.

Correspondence: Ying Poi Liu, uniQure biopharma B.V., Department of Research and Development, 1105 BP, Amsterdam, The Netherlands.
E-mail: y.poiliu@uniqure.com

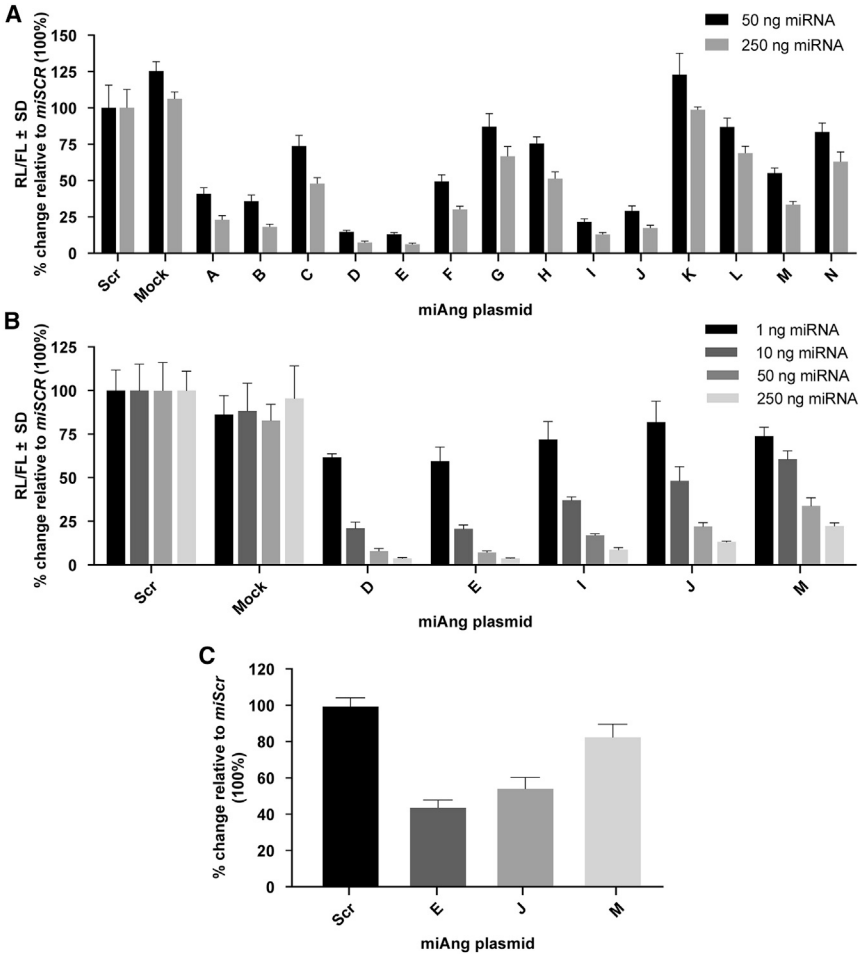

Figure 1. Dose-dependent knockdown of *ANGPTL3* gene expression by *miAngA* to *N*

(A and B) Luciferase activity in Huh7 cells co-transfected with *LucAng* and *miAng* or *miSCR* plasmids, and (C) endogenous *ANGPTL3* mRNA in Huh7 cells transfected with *miAng* or *miSCR* plasmids. For (A) and (B), the relative mean (±SD) luciferase activity was calculated as the ratio between RL and FL activities (n = 3–5). For (C), *ANGPTL3* mRNA levels in *miAng*-transfected cells are expressed as a percentage mean (±SD) relative to *miSCR*-transfected Huh7 cells (set to 100%, n = 2). FL, firefly luciferase; Luc, luciferase; miRNA, microRNA; RL, Renilla luciferase; SCR, scrambled control.

and the first phase I/II clinical study for miQURE-based therapy (NCT04120493) was initiated in 16 patients with HD in September 2019.[26] rAAV5 vectors have emerged as leading candidates for liver-directed AAV gene therapy, with numerous studies demonstrating the safety and efficacy of rAAV5-based gene therapies in people with hemophilia A and B.[27–32] The use of rAAV5-based miQURE technology for gene silencing in the liver has not yet been investigated. This proof-of-concept study uses dyslipidemia as an indication to investigate the safety and potency of liver-directed miQURE technology in mice. ANGPTL3 was selected as a target protein because it is almost exclusively expressed in the liver and because loss-of-function mutations in *ANGPTL3* and pharmacologic inactivation of ANGPTL3 protein are associated with low plasma levels of total cholesterol (TC), triglycerides (TG), and low-density lipoprotein (LDL),[33–35] all of which can be evaluated using established assays in a dyslipidemic APOE*3-Leiden.CETP mouse model.[34,36–39] This study shows that the potent knockdown of ANGPTL3 can be obtained using miQURE targeting *Angptl3*. Furthermore, miQURE expression following rAAV5 delivery led to significant reductions in TC and TGs with improvements in atherosclerosis in dyslipidemic mice. Overall, these results support the future development of miQURE technology to treat liver-directed diseases characterized by elevated levels of specific proteins.

RESULTS

In vitro screening of miRNA constructs targeting *ANGPTL3*

In total, 14 miRNA guide strands (designated *miAngA to miAngN*) were designed, spanning four *ANGPTL3* mRNA sequences conserved in humans, mice, rats, and non-human primates (NHPs). *miAngA-G* targeted the first part of exon 1, *miAngH-J* targeted the second part of exon 1, *miAngK-L* targeted exon 3, and *miAngM-N* targeted exon 5. Co-transfection of human hepatocellular (Huh7) cells with *miAng* and luciferase reporter (*LucAng*) plasmids identified four constructs (*miAngD, E, I,* and *J*) that induced >70% luciferase knockdown and six constructs achieving 25% to 65% knockdown (Figure 1A). Further testing of the most potent constructs targeting each sequence showed that luciferase knockdown was dose-dependent and that the order of potency was *miAngE* and *D*, followed by *miAngI, J*, and *M* (Figure 1B). Further studies excluded *miAngI* due to a single nucleotide mismatch between human and rodent sequences that precludes testing in mice. *miAngD* was excluded because it targets the same region of exon 1 as *miAngE*.

The greatest reduction in *ANGPTL3* mRNA expression in *miAng*-transfected Huh7 cells was observed for *miAngE*, followed by *miAngJ* and *M* (approximately −60%, −50%, and −20% knockdown, respectively) (Figure 1C). Results were similar irrespective of whether cells were transfected with 250 ng or 400 ng of plasmid (data not shown). Overall, *miAngE* was the second most abundant mature *miRNA* in *miAngE*-transfected Huh7 cells after miR-21, with processed forms accounting for 3.7% and 4.9% of the total annotated reads following transfection with 250 ng and 400 ng of plasmid, respectively (Figures S1A and S1B). The most abundant form of processed *miAngE in vitro* was 23 or 24 nucleotides long, depending on the experiment rather than the dose.

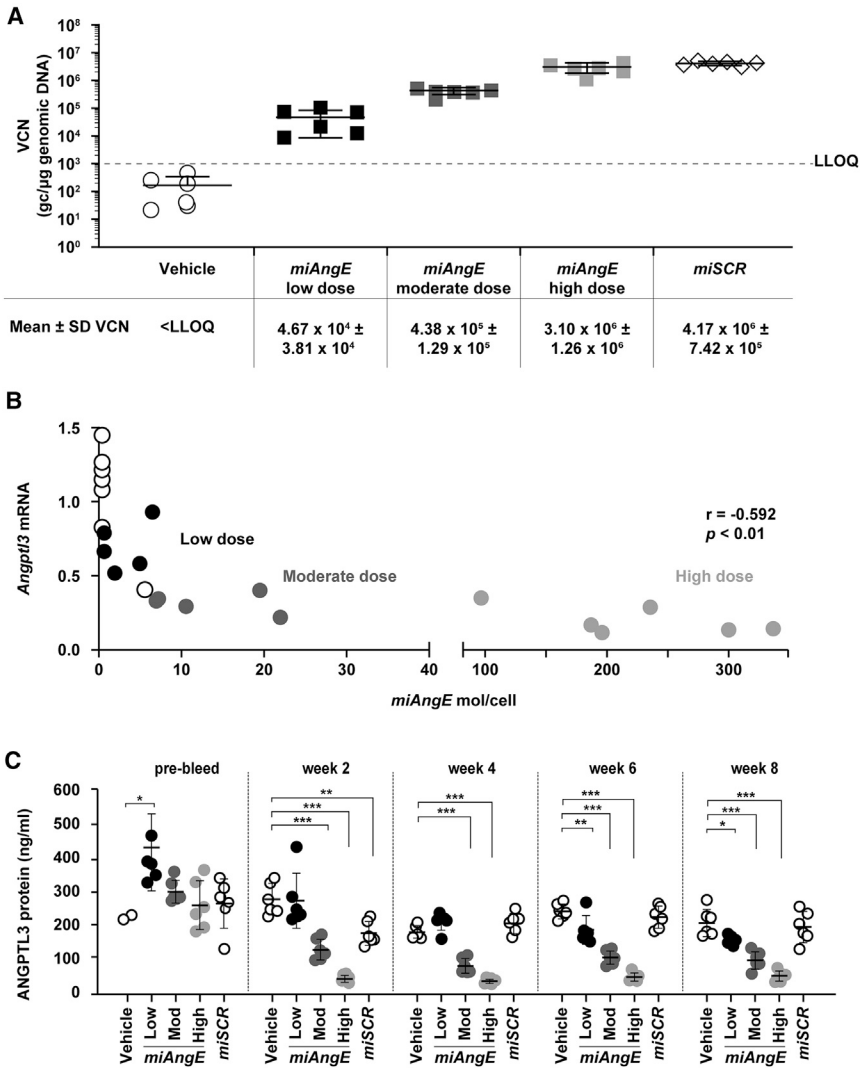

Figure 2. Vector DNA, *Angptl3* mRNA and ANGPTL3 protein quantification in liver or plasma of WT mice treated with vehicle, rAAV5-*miAngE* or rAAV5-*miSCR*

(A) Vector DNA copy numbers in liver tissue, (B) correlation between *Angptl3* mRNA and mature 23 nucleotide *miAngE* expression levels, and (C) changes in plasma ANGPTL3 protein levels over time in WT mice injected with vehicle control; low-, moderate-, or high-dose rAAV5-*miAngE;* or rAAV5-*miSCR*. Low dose, 1×10^{13} gc/kg; moderate dose, 5×10^{13} gc/kg; high dose, 2.5×10^{14} gc/kg; control, treatment-naïve plasma. VCN, vector copy number, are shown as genome copies per µg genomic DNA. GC, genome copies; rAAV5, recombinant adeno-associated virus serotype 5; WT, wild type. For (B), Pearson r was computed for X vs. every Y dataset. Pearson correlation calculations were based on the assumption that both X and Y values were sampled from populations that follow a Gaussian distribution. Two-tailed p value and 95% confidence intervals were used (GraphPad Prism 8.0.0). For (C), significant changes vs. vehicle control were determined using one-way ANOVA, Bonferroni post-test (GraphPad Prism 8.0.0). Mean is (± SD). *p < 0.05; **p < 0.01; ***p < 0.001. LLOQ, lower limit of quantification. In (C), one deviating value in the pre-bleed dataset (which is therefore not related to treatment) has been removed to allow the data to be better visualized on the Y scale.

rAAV5-miAngE dose-dependently reduces *Angptl3* mRNA and ANGPTL3 protein levels in WT mice, without safety concerns

The most potent miRNA candidate (*miAngE*) *in vitro* was selected for dose-response studies in wild-type (WT) mice (low dose: 1×10^{13} gc/kg; moderate dose: 5×10^{13} gc/kg; high dose: 2.5×10^{14} gc/kg). All animals survived post-injection. Mean liver VCNs in mice injected with rAAV5-*miAngE* or a high dose (2.5×10^{14} gc/kg) of rAAV5-*miSCR* control (rAAV5 encoding a scrambled *Angptl3* targeting miRNA) were dose-dependent for each treatment group, indicating that the injection procedures were performed correctly in all mice (Figure 2A). Dose-dependent reductions in liver *Angptl3* mRNA levels were detected following rAAV5-*miAngE* injection, ranging from −77% in the high-dose group vs. vehicle control, followed by −60% and −25% in the moderate- and low-dose groups, respectively (data not shown). Although *Angptl3* mRNA expression increased by +40% in animals injected with rAAV5-*miSCR* vs. vehicle control, results in both control groups were highly variable, while liver ANGPTL3 protein levels remained constant. Consistent with vector DNA and mRNA results, significant dose-dependent increases in mature *miAngE* were detected in liver (Figure 2B) that corresponded with significant reductions in plasma ANGPTL3 protein levels from week 2–8 (Figure 2C). Prior to treatment, significant differences in plasma ANGPTL3 levels were only observed between mice assigned to the vehicle group and those assigned to low-dose treatment. At week 2, up to −90% ANGPTL3 protein knockdown vs. vehicle control was detected in the high-dose group, with approximately −50% and −25% knockdown in the moderate- and low-dose groups, respectively. No changes in liver function enzymes were observed in WT mice treated with rAAV5-*miSCR* or low- to moderate-dose rAAV5-*miAngE*. Although small transient increases in plasma alanine aminotransferase (ALT) and aspartate transaminase (AST) activity (<2.5-fold increases affecting one and three mice, respectively) were observed at a single time point (4 weeks post-treatment) in the high-dose group and the *miSCR* group (Table 1), no macroscopic abnormalities in organ morphology (including the liver) were detected after animals were euthanized.

rAAV5-miAngE induces Angptl3 knockdown in dyslipidemic mice treated with or without atorvastatin, without safety concerns

Based on results in WT mice, a moderate-high dose of AAV5-*miAngE* (1×10^{14} gc/kg) was selected for further studies in

Table 1. Changes over time in mean plasma ALT and AST activity in WT mice injected with vehicle control; low-, moderate-, or high-dose rAAV5-*miAngE;* or rAAV5-*miSCR*

	Mean (±SD) ALT activity (mU/mL)			Mean (±SD) AST activity (mU/mL)		
	Week 2	Week 4	Week 8	Week 2	Week 4	Week 8
Vehicle	4.98 ± 0.54	4.23 ± 0.54	6.85 ± 0.45	25.66 ± 7.40	21.66 ± 5.08	27.15 ± 7.94
rAAV5-*miSCR*	5.38 ± 0.67	5.53 ± 0.75	8.13 ± 1.48	28.15 ± 5.99	21.09 ± 1.91	29.01 ± 12.68
Low-dose rAAV5-*miAngE*	4.46 ± 0.51	4.73 ± 0.84	7.52 ± 0.70	30.03 ± 8.50	25.41 ± 8.53	26.26 ± 7.54
Moderate-dose rAAV5-*miAngE*	4.49 ± 0.47	4.73 ± 0.89	6.82 ± 0.82	24.90 ± 5.03	21.60 ± 3.43	22.42 ± 6.49
High-dose rAAV5-*miAngE*	5.71 ± 1.78	5.81 ± 1.56	7.19 ± 0.87	31.11 ± 14.55	35.93 ± 16.73 *	25.56 ± 7.76

Low dose, 1×10^{13} gc/kg; moderate dose, 5×10^{13} gc/kg; moderate-high dose, 1×10^{14} gc/kg; high dose, 2.5×10^{14} gc/kg. ALT, alanine aminotransferase; AST, aspartate transaminase; rAAV5, recombinant adeno-associated virus serotype 5. Mean is (±SD). *$p \leq 0.05$ (ANOVA and Dunnett).

dyslipidemic APOE*3-Leiden.CETP mice treated with and without atorvastatin. The APOE*3-Leiden.CETP mouse model was chosen for these studies because it is a well-established model for hyperlipidemia and atherosclerosis with humanized lipoprotein metabolism that responds to all known therapeutic interventions currently used in the clinic.[34,36–39] All animals survived post-injection. Mean liver VCNs in rAAV5-*miAngE,* and rAAV5-*miSCR*-injected mice were similar within each treatment group irrespective of atorvastatin treatment (Figure 3A). As expected, quantifiable levels of mature *AngE* miRNA (23 nucleotide variant) were detected only in the rAAV5-*miAngE* injected groups, with an average of 87 and 107 molecules/cell in groups receiving rAAV5-*miAngE* alone and in combination with atorvastatin, respectively (data not shown). Reductions in *Angptl3* mRNA expression in livers were similar for mice treated with rAAV5-*miAngE* with and without atorvastatin (−30% vs. vehicle control and −40% vs. rAAV5-*miSCR)* (Figure 3B). However, results were not statistically significant due to variability in *Angplt3* mRNA expression within control groups. Levels of ANGPTL3 protein in liver were significantly reduced by −27% and −21% vs. vehicle control with rAAV5-*miAngE* + atorvastatin and rAAV5-*miSCR* + atorvastatin, respectively, and by −25% and −19% vs. rAAV5-*miSCR* with rAAV5-*miAngE* + atorvastatin and rAAV5-*miSCR* + atorvastatin, respectively (Figure 3C). Plasma levels of ANGPTL3 protein in rAAV5-*miAngE* treated mice were significantly reduced throughout the study, with a maximum silencing effect (−77% vs. both control groups) at week 4 (Figure 3D). Atorvastatin had no impact on levels of ANGPTL3 protein in rAAV5-*miAngE*-treated mice. All mice appeared healthy and behaved normally with no signs of discomfort and no treatment-related changes in body weight (Figure S2A), food intake (Figure S2B), or liver tissue weight. Analyses of pooled plasma samples from mice treated with rAAV5-*miRNA* alone showed that levels of ALT and AST were within the normal range (<2.5-fold increase) throughout the study with no difference compared with vehicle-treated controls (Table 2). Toxicologic profiling showed no impact for any intervention on plasma levels of total protein, urea, creatinine, glucose, or phospholipids, and histopathological analysis showed no effects on heart apex, liver, spleen, pancreas, brain, kidney, lung, ovaries, and adrenal gland tissues. Livers appeared pale for most mice irrespective of treatment group, with signs of diffuse hepatocellular rarefactions, micro- and macro-vesicular vacuolation, and hepatocellular inclusions consistent with hepatic steatosis and/or non-alcoholic fatty liver disease (NAFLD) resulting from the high-fat (0.15% cholesterol/15% TG) Western-type diet (WTD) diet. No off-target effects were observed in rAAV5-*miAngE*-treated mice. Differentially expressed gene (DEG) profiles in liver tissue were similar for both control groups (vehicle vs. rAAV5-*miSCR*); this was also true of rAAV5-*miAngE* vs. rAAV5-*miSCR* excepting the upregulation of one gene (predicted Gm11189 pseudogene) in rAAV5-miAngE-treated mice (Figure S3). Furthermore, Reactome pathway (Figure S4) and Gene Ontology (GO) (Figure S5) analysis (rAAV5-*miAngE* vs. rAAV5-*miSCR*) revealed no significant enrichment of any pathways or terms, respectively, confirming that rAAV5-*miAngE* transduction was not driving hepatotoxic effects such as an inflammatory response.

rAAV5-miAngE improves lipid profile in dyslipidemic mice treated with or without atorvastatin

Plasma TC levels in dyslipidemic mice were significantly reduced 2 to 16 weeks after treatment with a moderate-high dose of rAAV5-*miAngE* (1×10^{14} gc/kg) co-administered with and without atorvastatin (Figure 4A; Tables S1 and S2). Reductions with rAAV5-*miAng*E alone ranged from −30% to −58% vs. vehicle control and from −37% to −60% vs. rAAV5-*miSCR*. Comparable reductions when rAAV5-*miAngE* was co-administered with atorvastatin were −54% to −71% vs. vehicle control and −59% to −71% vs. rAAV5-*miSCR*. In comparison, TC levels were reduced by approximately −17% to −34% in rAAV5-*miSCR*-injected mice treated with atorvastatin from week 4 until week 16. Overall TC exposure was reduced by −41% and −58% in rAAV5-*miAngE* and rAAV5-*miAngE* + atorvastatin groups, respectively, vs. vehicle control, and by −46% and −61%, respectively, vs. rAAV5-*miSCR*. Plasma TG levels in dyslipidemic mice treated with rAAV5-*miAngE* alone were significantly reduced by −58% to −69% from week 2–12 vs. vehicle control and by −54% to −69% from week 2–14 vs. rAAV5-*miSCR* (Figure 4B; Tables S1 and S2). Comparable reductions in mice treated with rAAV5-*miAngE* + atorvastatin were −49% to −69% vs. vehicle control and −52% to −70% vs. *miSCR*. TG reductions were not significant at weeks 14 or 16 vs. vehicle or at week 16 vs. *miSCR*, irrespective of whether rAAV5-*miAng*E was administered with or without

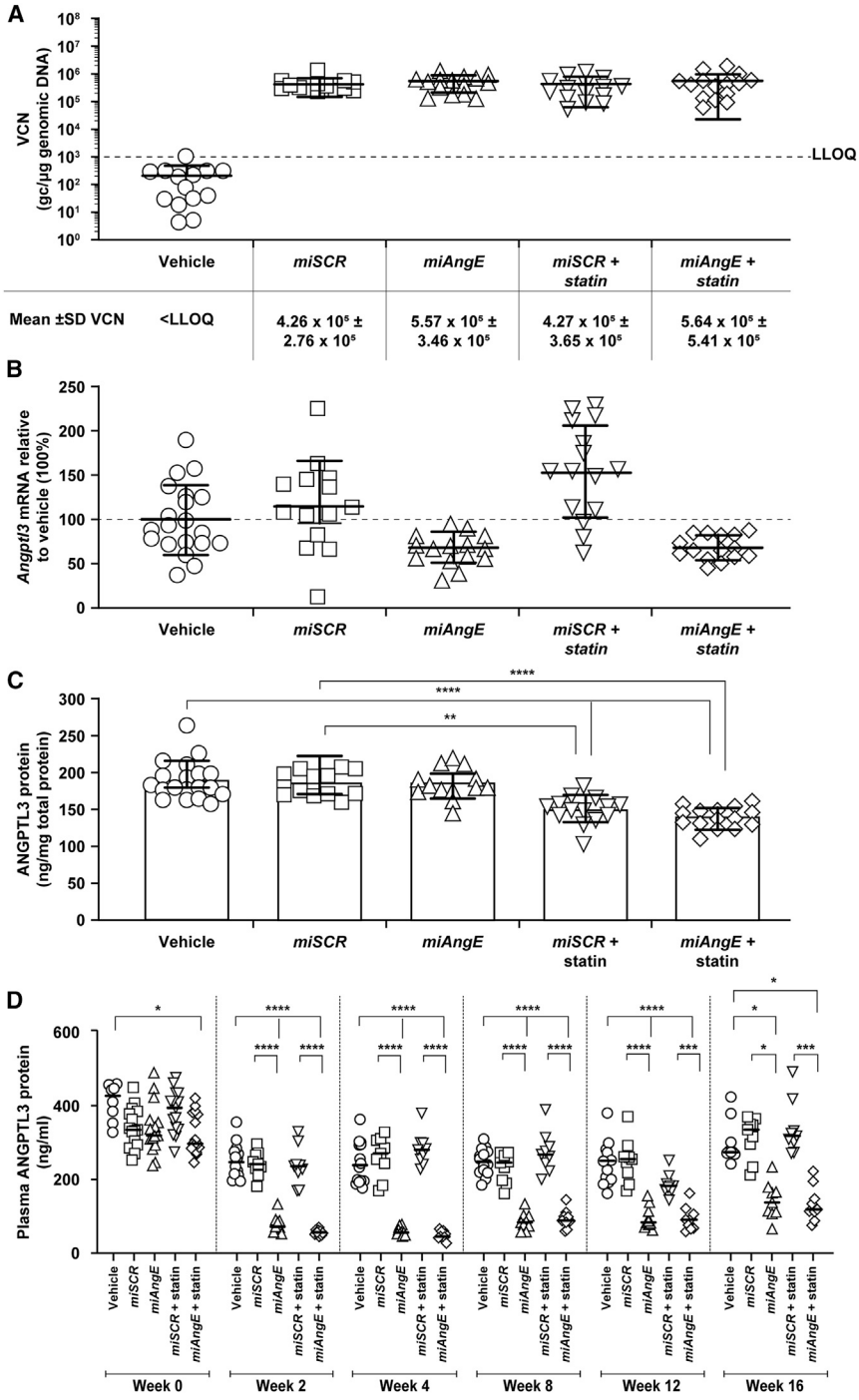

Figure 3. Vector DNA, *Angptl3* mRNA and ANGPTL3 protein quantification in liver and/or plasma of dyslipidemic APOE*3-Leiden.CETP mice treated with vehicle, rAAV5-*miSCR* or rAAV5-*miAngE* (with or without atorvastatin)

(A) Vector DNA copy numbers in liver, (B) percent change in liver *Angptl3* mRNA levels relative to vehicle control, (C) changes in liver ANGPTL3 protein levels vs. vehicle or *miSCR* controls, and (D) changes in plasma ANGPTL3 protein levels vs. vehicle or *miSCR* controls in dyslipidemic APOE*3-Leiden.CETP mice injected with moderate-high dose rAAV5-*miAngE* or rAAV5-*miSCR*, with or without atorvastatin. For (A)–(C), analyzed samples are vehicle group n = 20, *miSCR* group n = 15, miAngE group n = 15, *miSCR* + statin n = 15, *miAngE* + statin n = 15. For (D), week 0 analyzed samples vehicle group n = 8, *miSCR* group n = 15, miAngE group n = 15, *miSCR* + statin n = 15, *miAngE* + statin n = 15; for (D), week 2–16 analyzed samples vehicle group n = 14 (except week 16 n = 9), *miSCR* group n = 9, *miAngE* group n = 9, *miSCR* + statin n = 9, *miAngE* + statin n = 9. The p values for (C) and (D) were calculated using one-way ANOVA, Bonferroni post-test. Moderate-high dose,1 × 10^{14} gc/kg of rAAV5-*miAngE* or rAAV5-*miSCR*. Control, treatment-naïve plasma; GC, genome copies; LLOQ, lower limit of quantification; rAAV5, recombinant adeno-associated virus serotype 5. Mean is (± SD). *p < 0.05; **p < 0.001; ***p = 0.0007; ****p < 0.0001.

atorvastatin. Overall, TG exposure was reduced by −58% and −51% vs. vehicle control in rAAV5-*miAngE* and rAAV5-*miAngE* + atorvastatin groups, respectively, and by −58% and −55%, respectively, vs. *miSCR*. Analyses of lipoprotein profiles at the study endpoint showed that the significant decreases in TC and TG in mice treated with rAAV5-*miAngE* primarily occurred in non-high-density lipoprotein (HDL) (very low-density lipoprotein [VLDL] and LDL) fractions, irrespective of whether mice were co-treated with atorvastatin (Figures 5A and 5B). HDL was largely unchanged in all profiles. Lipoprotein profiles at week 8 are shown in Figure S6.

rAAV5-miAngE reduces atherosclerosis progression in dyslipidemic mice treated with or without atorvastatin

Moderate-high dose rAAV5-*miAngE* (1 × 10^{14} gc/kg) reduced total atherosclerotic lesion area in dyslipidemic mice by −53% vs. vehicle control and by −58% vs. rAAV5-*miSCR* (Figure 6A). Reductions when rAAV5-*miAngE* was co-administered with atorvastatin were −84% and −86% vs. vehicle and *miSCR* controls, respectively, and −66% vs. rAAV5-*miAngE* alone. Treatment with rAAV5-*miAngE* alone or in combination with atorvastatin was associated with the maintenance of an undiseased plaque phenotype and fewer severe type IV and V lesions vs. both control groups (Figure 6B). Treatment with rAAV5-*miAngE* + atorvastatin combined provided additional preservation of normal aortic root sections and a further reduction in the development of severe (type IV and V) lesions compared with rAAV5-*miAngE* (Figure 6C).

Table 2. Changes over time in mean plasma ALT and AST activity in dyslipidemic mice injected with vehicle control, moderate-high dose rAAV5-*miAngE*, or rAAV5-*miSCR*, with or without atorvastatin treatment

	Mean (SD) ALT activity (mU/mL)				Mean (SD) AST activity (mU/mL)			
	Week 4 (n = 6)	Week 8 (n = 6[a])	Week 12 (n = 6[b])	Week 16 (n = 6)	Week 4 (n = 6)	Week 8 (n = 6[c])	Week 12 (n = 6[b])	Week 16 (n = 6)
Vehicle	84.2 ± 29.7	54.8 ± 10.9	69.3 ± 39.3	85.7 ± 53.5	161.3 ± 55.8	121.9 ± 26.6	187.7 ± 85.0	196.7 ± 155.2
rAAV5-*miSCR*	66.0 ± 12.5	57.2 ± 8.0	47.9 ± 15.9	59.8 ± 26.4	139.1 ± 33.9	151.2 ± 25.3	144 ± 30.3	146.8 ± 63.3
Moderate-high dose rAAV5-*miAngE*	132.0 ± 51.5	73.3 ± 21.8	81.7 ± 53.8	96.5 ± 40.9	230.9 ± 76.2	173.9 ± 49.2	198.4 ± 93.9	204.3 ± 87.0
rAAV5-*miSCR* + statin	91.0 ± 33.8	87.8 ± 77.1	102.8 ± 111,5	106.2 ± 119.0	188.7 ± 69.9	193.3 ± 135.9	235.8 ± 184.2	233.5 ± 206.0
Moderate-high dose rAAV5-*miAngE* + statin	109.8 ± 51.6	94.4 ± 38.6	101.2 ± 56.9	355.8 ± 366.2	225.4 ± 109.1	192.8 ± 70.8	243.8 ± 120.4	355.8 ± 366.2

[a]n = 4 for the vehicle control group.
[b]n = 5 for the moderate-high dose group.
[c]n = 5 for the vehicle control group. Low dose, 1×10^{13} gc/kg; moderate dose, 5×10^{13} gc/kg; moderate-high dose, 1×10^{14} gc/kg; high dose, 2.5×10^{14} gc/kg. p values for each group vs. vehicle control were not significant (ANOVA and Dunnett). Mean is (±SD). ALT, alanine aminotransferase; AST, aspartate transaminase; rAAV5, recombinant adeno-associated virus serotype 5.

DISCUSSION

The ability of RNAi to modulate gene expression and its potential as a therapeutic tool has been conclusively demonstrated.[40–42] Early barriers to the successful translation of RNAi triggers, such as miRNAs, to the clinic (e.g., off-target activity, systemic delivery, and persistence) have been addressed by numerous innovative designs.[40,43] Currently, engineered miRNA-based therapies are undergoing evaluation in phase I/II clinical trials for diseases such as hepatitis C, liver and kidney dysfunction, and various cancers.[41,44] miQURE is an miRNA delivery platform that uses an miR-451 scaffold to limit off-target effects and toxicity,[16–18] and an rAAV vector to enhance the delivery and durability of therapeutic miRNAs.[5,12,22,23] Here, we evaluate the safety and efficacy of miQURE technology, which is used to deliver therapeutic miRNA for liver-specific indications.

Overall, 14 candidate *miRNA* constructs were designed targeting four regions of the *ANGPTL3* mRNA, and the most potent candidate (*miAngE*) *in vitro* was used for dose-response studies in WT mice and for lipid-lowering studies in dyslipidemic APOE*3-Leiden.CETP mice. rAAV5-*miAngE* dose-dependently and significantly reduced *Angptl3* mRNA expression in the livers of WT mice by > −70%, −60%, and −25% vs. vehicle control at high, moderate, and low doses (2.5×10^{14}, 5×10^{13} and 1×10^{13} gc/kg), respectively, whereas the reduction was less marked (−30%) in cholesterol- and fat-fed dyslipidemic mice receiving moderate-high dose (1×10^{14} gc/kg) rAAV5-*miAngE*. In addition, treatment with rAAV5-*miAngE* markedly reduced atherosclerosis development when administered alone, with greater reductions when rAAV5-*miAngE* was co-administered with atorvastatin. Compared with a chow diet, the diet used in this study induces an approximate 7- and 3-fold increase in hepatic levels of cholesterol esters and TG, respectively, in female APOE*3-Leiden.CETP mice.[45] Moreover, previous studies (supported by histopathology findings in the current study) show that APOE*3-Leiden.CETP mice fed with a high-fat diet develop hepatic steatosis and/or NAFLD.[46] This is important because correlations have been reported between markers of liver damage (AST/ALT elevations and cytotoxic T cell immune responses) and reductions in transgene expression following gene therapies based on AAV serotypes 2, 8, and 10.[47–49] However, no associations have been demonstrated between liver damage markers and transgene expression in clinical trials for AAV5-based gene therapy,[31,50,51] and the current study found that mean VCNs (an indicator of transduction efficacy) following rAAV5-*miAngE* injection were dose-dependent in WT and dyslipidemic mice (4.38×10^5 and 3.10×10^6 gc/μg genomic DNA with moderate and high doses in WT mice, respectively, and 5.57×10^5 gc/μg with the moderate-high dose in dyslipidemic mice). This, together with variations in *Angptl3* mRNA expression within vehicle and rAAV5-*miSCR* control groups, suggests the discrepancy between WT and dyslipidemic mice is most likely explained by variability in levels of endogenous *Angptl3* mRNA expression rather than differences in rAAV5 transduction efficacy in healthy vs. fatty livers. Moreover, plasma levels of ANGPTL3 protein were dose-dependently reduced across studies, with maximum reductions of −50% and −90% with moderate- and high-dose rAAV5-*miAngE*, respectively, in WT mice and −77% with the moderate-high dose in dyslipidemic mice. As expected, atorvastatin had no impact on ANGPTL3 protein levels in dyslipidemic mice. ANGPTL3 prevents the hydrolysis of TG in VLDL and, consequently, VLDL clearance by inhibiting lipoprotein lipase (LPL) activity while promoting HDL remodeling by reducing endothelial lipase activity.[33,52] Consequently, loss-of-function ANGPTL3 variants and inhibition of ANGPTL3 using evinacumab are associated with low levels of plasma TGs and VLDL-C/LDL-C, moderately low levels of HDL-C and reduced cardiovascular risk.[34,35,52,53] As expected, mean plasma levels of TG and TC were significantly reduced in dyslipidemic mice receiving moderate-high dose rAAV5-*miAngE*, with a −70% reduction in TG vs. both controls at weeks 2–12 and a −60% reduction in TC at weeks 2–16. Slight elevations in TC and TG levels toward the end of the study corresponded with slightly higher levels of ANGPTL3 protein compared with previous timepoints and may be due to the induction of feedback mechanisms responding to earlier reductions in

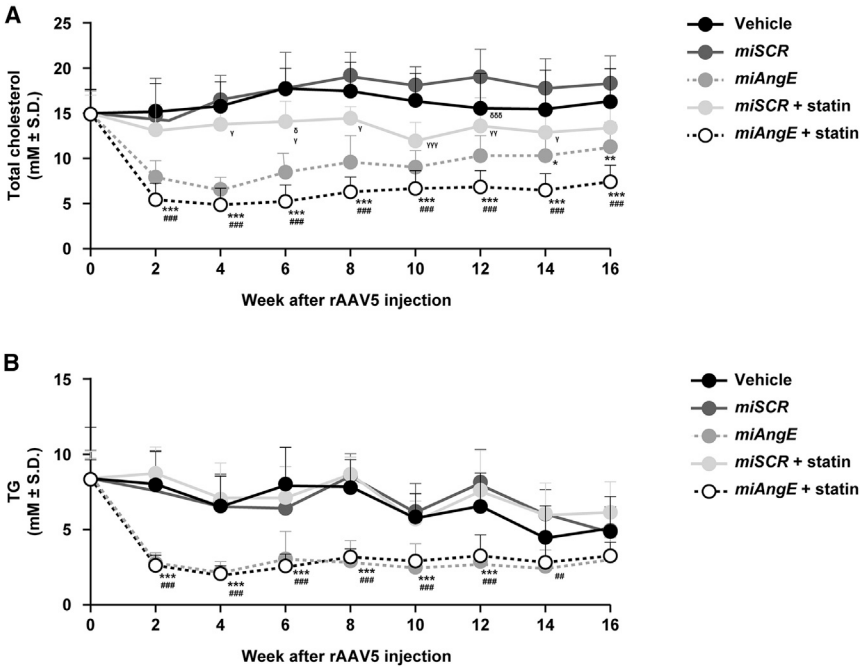

Figure 4. Plasma total cholesterol and triglycerides levels in dyslipidemic APOE*3-Leiden.CETP mice treated with vehicle, rAAV5-*miSCR* or rAAV5-*miAngE* (with or without atorvastatin)

Changes over time in mean (±SD) plasma levels of (A) total cholesterol and (B) triglycerides in dyslipidemic APOE*3-Leiden.CETP mice injected with vehicle control, moderate-high dose rAAV5-*miAngE,* or rAAV5-*miSCR*, with and without atorvastatin. The p values were calculated using one-way ANOVA, Bonferroni post-test. Moderate-high dose (1×10^{14} gc/kg) of rAAV5-miAngE or rAAV5-miSCR. Atorvastatin dose 45 mg/kg rAAV5, recombinant adeno-associated virus serotype 5. Mean is (±SD). *p < 0.05 *miAngE* vs. vehicle; **p < 0.01 *miAngE* vs. vehicle; ***p < 0.001 *miAngE* (up to week 12) and *miAngE* + atorvastatin vs. vehicle; $^{\#\#\#}$p < 0.001 *miAngE* and *miAngE* + atorvastatin vs. *miSCR;* $^{\#\#}$p < 0.01 *miAngE* and *miAngE* + atorvastatin vs. *miSCR;* $^{\delta}$p < 0.05 *miSCR*+ atorvastatin vs. vehicle; $^{\delta\delta\delta}$p < 0.001 *miSCR*+ atorvastatin vs. vehicle; $^{\gamma}$p < 0.05 *miSCR*+ atorvastatin vs. *miSCR;* $^{\gamma\gamma}$p < 0.001 *miSCR*+ atorvastatin vs. *miSCR.*

TG and TC. However, longer-term studies are required to assess the durability of miQURE technology targeting the liver. Most of the changes in TG and TC occurred in the atherogenic apoB-containing VLDL-LDL fractions, with very few changes in HDL particles. Treatment guidelines for dyslipidemia recommend lifestyle modification with or without pharmacotherapy (usually a statin) to lower plasma LDL-C levels to specific targets, thereby reducing cardiovascular risk.[54,55] As expected, the current study found that co-administration of atorvastatin with rAAV5-*miAngE* in dyslipidemic APOE*3-Leiden.CETP mice led to greater TC reductions than those achieved with either treatment alone, whereas the significant reductions in TG achieved using rAAV5-*miAngE* were similar irrespective of atorvastatin treatment. Overall, dyslipidemic mice treated with rAAV5-*miAngE* plus atorvastatin showed greater reductions in atherosclerosis progression, increased numbers of undiseased segments, and reduced lesion severity vs. either treatment alone. While this can be partly explained by the beneficial changes in lipid profile, previous studies show that the anti-inflammatory effects of statins contribute to cardiovascular risk reduction by stabilizing the atherosclerotic plaque and slowing atherosclerosis progression.[56]

An engineered siRNA (ANGsiR10) designed to degrade *ANGPTL3* mRNA, which is hepatocyte targeted by N-acetylgalactosamine (GalNAc) conjugation, has recently been reported to maximally lower plasma TG and cholesterol levels in dyslipidemic (hApoC3-Tg) mice, by ~96% and ~75%, respectively, over 14 weeks.[57] The lipid-lowering effects of ANGsiR10 are comparable to those obtained with rAAV-*miAngE* in terms of magnitude (maximal lowering of plasma TG and TC [rAAV5- *miAngE* vs. rAAV5-*miSCR*] of 69% and 60%, respectively) and duration of lipid-lowering (14–16 weeks in this study). However, the endpoints used (e.g., lipid levels, the ratio of ApoA and B, and lipid deposition in the liver) were not as comprehensive as those used in this study, given that histological evaluation of atherosclerosis in the vasculature was not undertaken.

Treatment of WT and dyslipidemic mice with rAAV5-*miRNA* was generally safe and well-tolerated. As expected, ALT/AST levels were slightly higher in APOE*3-Leiden.CETP mice fed on a WTD than in WT mice fed on a chow diet. Although small elevations in ALT and AST levels (markers of liver function) were observed in WT mice treated with high-dose rAAV5-*miAngE* (1.24- and 1.66-fold increases, respectively, vs. vehicle control) at a single time point (week 4), elevations were transient and were not associated with changes in liver morphology. Similar transient and asymptomatic elevations in liver transaminases have previously been observed after administration of AAV vectors in clinical trials for hemophilia B.[58,59] The wide range of AST/ALT activities between animals at week 4 and the fact that hepatocellular injury usually results in persistent, much higher (10- to 20-fold) elevations in AST/ALT[60] suggests that elevations were likely due to physiological variations between mice or assay-related differences rather than to changes in liver function. ALT/AST levels remained within normal limits throughout the studies for all other cohorts. This proof-of-concept study was designed to examine the potential use of miQURE technology for the treatment of liver-directed disorders using rAAV5-*miAng* constructs as a therapeutic research tool. Consequently, the safety profile of rAAV5-*miRNA* was not fully characterized. However, unpublished data show that *miAngE* expression levels in rAAV5-*miAngE*-treated mice were well within the range of endogenous miRNA expression, suggesting a low risk of interference with the endogenous RNAi pathway. Moreover, candidate *miAngs* were designed to specifically target *ANGPTL3* mRNA and exclude perfect binding with other target mRNAs to exclude off-target effects. This

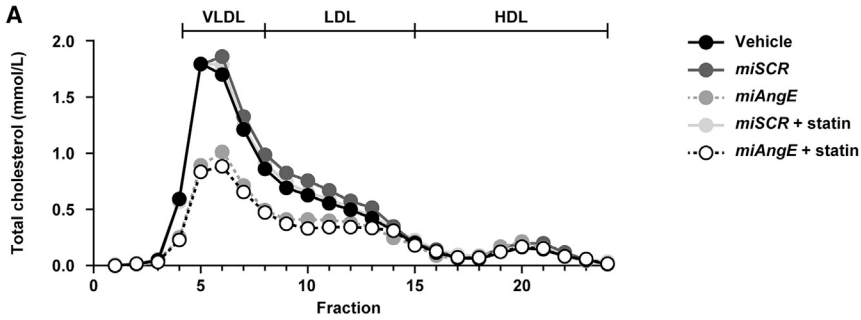

Total cholesterol (mmol/L)	Vehicle	miSCR	miAngE	miSCR + statin	miAngE + statin
VLDL (fractions 3-8)	6.240	6.477	3.396	6.400	3.095
LDL (fractions 9-17)	3.545	4.347	2.635	3.905	2.476
HDL (fractions 18-24)	0.696	0.988	0.870	0.832	0.831

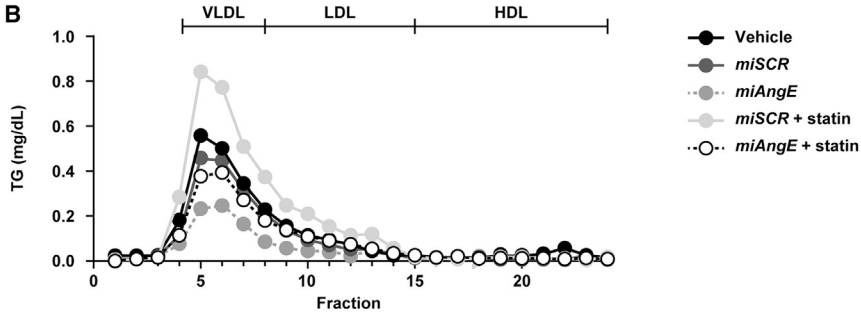

Total TG (mg/L)	Vehicle	miSCR	miAngE	miSCR + statin	miAngE + statin
VLDL (fractions 3-8)	1.841	1.534	0.812	2.804	1.308
LDL (fractions 9-17)	0.559	0.429	0.211	0.923	0.475
HDL (fractions 18-24)	0.184	0.016	0.003	0.003	0.008

Figure 5. Lipid profiles for cholesterol and triglycerides in dyslipidemic APOE*3-Leiden.CETP mice treated with vehicle, rAAV5-*miSCR* or rAAV5-*miAngE* (with or without atorvastatin)

Lipid profiles for (A) cholesterol and (B) triglycerides in dyslipidemic APOE*3-Leiden.CETP mice 16 weeks after treatment with vehicle control, moderate-high dose rAAV5-*miAngE* or rAAV5-*miSCR*, with and without atorvastatin. For (A) and (B), dots represent the mean value of the group per fraction (n = 9 per treatment group). Moderate-high dose (1×10^{14} gc/kg) of rAAV5-*miAngE* or rAAV5-*miSCR*. Atorvastatin dose 45 mg/kg. Tables in (A) and (B) give the area under the curve for fractions 3–8 VLDL, 9–17 LDL, and 18–24 HDL at t = 16 for indicating their cholesterol and triglycerides content, respectively, for each experimental treatment. HDL, high-density lipoprotein; LDL, low-density lipoprotein; rAAV5, recombinant adeno-associated virus serotype 5; TG, triglyceride; VLDL, very low-density lipoprotein.

is because perfectly complementary mature miRNAs cause mRNA cleavage, whereas partially complementary miRNAs can result in translational inhibition. As expected, no off-target effects were observed in mice. DEG profiles in liver tissue from dyslipidemic mice were similar for both control groups (vehicle vs. rAAV5-*miSCR*); this was also true of rAAV5-*miAngE* vs. rAAV5-*miSCR* excepting the upregulation of one gene (predicted Gm11189 pseudogene) in rAAV5-*miAngE*-treated mice. Finally, miQURE technology requires a one-time administration, whereas transient RNAi-based treatments require repeated dosing that may be associated with adverse events.

In conclusion, this is the first study to show that miQURE technology effectively transduces the liver following a one-time intravenous (i.v.) administration in mice with healthy and diseased livers leading to dose-dependent reductions in target mRNA and protein knockdown with no safety signals. Overall, results support the development of miQURE technology for the treatment of liver-based disorders characterized by elevated levels of disease-causing proteins.

MATERIAL AND METHODS

In vitro studies

Construct design and production

Full-length *ANGPTL3* mRNA sequences for humans (GenBank: NM_014495), NHPs (GenBank: XM_005543185), mice (GenBank: NM_013913), and rats (GenBank: NM_001025065.1) were aligned using the Log-Expectation (MUSCLE) alignment tool with default settings (https://www.ebi.ac.uk/Tools/msa/muscle/). Conserved sequences were identified and used to design candidate *miAng* guide strands. A negative control (*miSCR*) was created by scrambling *miAng* sequences using GenScript software (https://www.genscript.com/tools/create-scrambled-sequence). *miAng* and *miSCR* control sequences were embedded in the human pre-miR-451 scaffold, flanked by 90 nucleotides of the 5′ and 3′ ends containing *AscI* and *NotI* restriction sites, and complete sequences were synthesized by GeneArt (Invitrogen, Thermo Fisher Scientific). Pri-*miAng* cassettes were expressed from the HCR-hAAT promoter (the apolipoprotein E locus control region, human alpha1-antitrypsin) and terminated by the SV40 polyA signal. Two firefly luciferase (FL) reporter plasmids were generated by combining sequences within *Angptl3* exons 1, 3, 4, and 5 (*LucAngA)* or exons 6 and 7 (*LucAngB*) with 5′ and 3′ flanking regions containing *AscI* and *NotI* restriction sites and the 3′UTR of the *Renilla Luciferase (RL)* gene in the psiCHECK-2 vector (Promega, Thermo Fisher Scientific). Sequences were synthesized and plasmids were cloned by GeneArt (Invitrogen, Thermo Fisher Scientific). The secondary structure of the RNA transcripts was predicted using the mfold program.[61]

Analysis of miAng-mediated luciferase knockdown

Huh-7 cells were co-transfected in P24-well plates in triplicate with 50 ng *LucAngA* or *LucAngB* and 50 ng or 250 ng of each *miAng*/*miSCR* plasmid using Lipofectamine 3000 reagent (Thermo Fisher Scientific). Transfected cells were collected 48 h post-transfection in passive lysis buffer (Promega, Thermo Fisher Scientific), and FL and RL activities were measured in cell lysates using the Dual-Luciferase Reporter Assay System (Promega, Thermo Fisher Scientific) according to the manufacturer's instructions. Relative luciferase activity was calculated, and factor corrected as the ratio

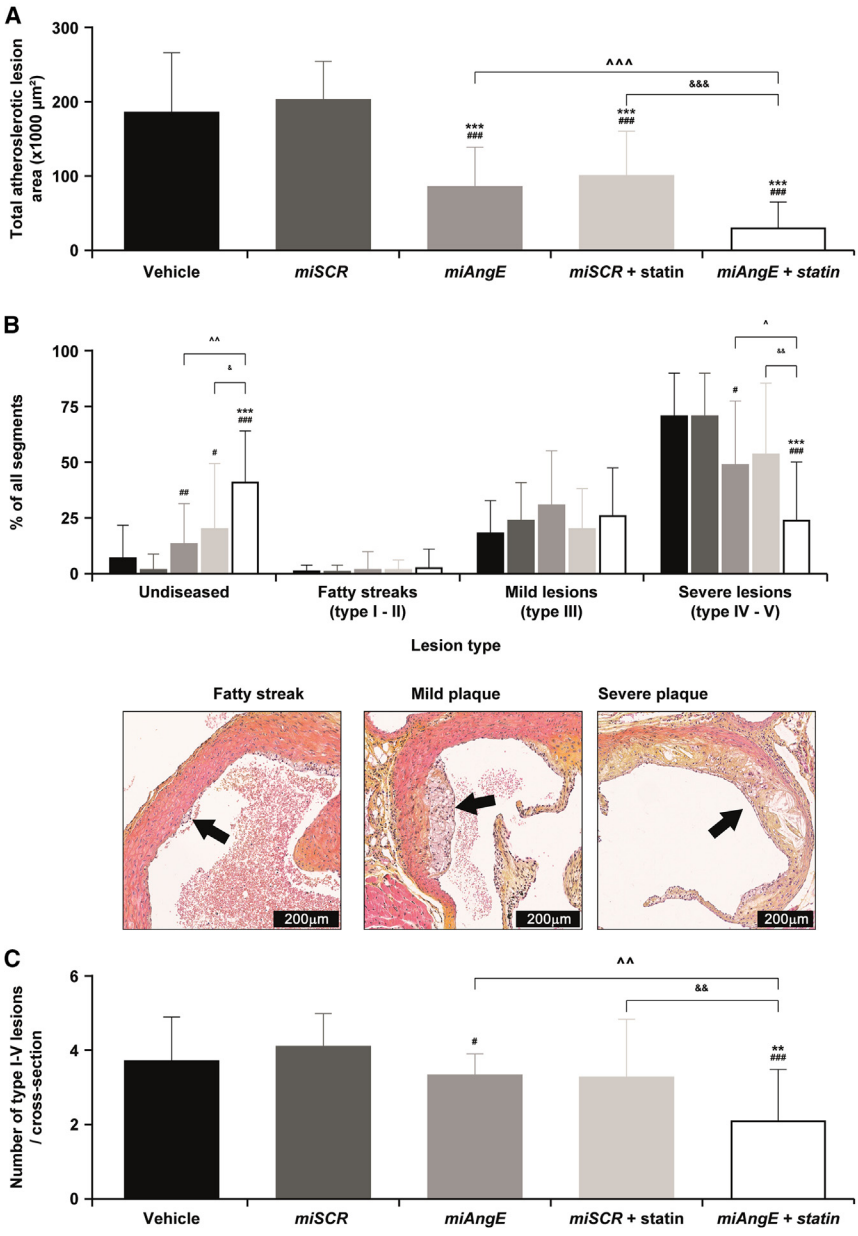

Figure 6. Atherosclerotic lesion area and lesion severity in dyslipidemic APOE*3-Leiden.CETP mice treated with vehicle, rAAV5-*miSCR* or rAAV5-*miAngE* (with or without atorvastatin)

(A) Total atherosclerotic lesion area, (B) severity of atherosclerotic lesions, and (C) number of total lesions per cross-section in dyslipidemic APOE*3-Leiden.CETP mice 16 weeks after treatment with vehicle control or moderate-high dose rAAV5-*miAngE* or rAAV5-*miSCR*, with or without atorvastatin treatment. Severity of atherosclerotic lesions is expressed as a percentage of all segments showing undiseased tissue or type I–V lesions. Representative pictures of a fatty streak, and mild and severe lesions are shown (original magnification ×20). Scale bar, 200 µm. Pink-purple are smooth muscle cells; yellow is connective tissue/collagen; white/translucent are lipid droplets in macrophages and cholesterol clefts. Statistical analyses were performed using a Kruskal-Wallis test followed by individual Mann-Whitney tests for group comparisons. Moderate-high dose (1×10^{14} gc/kg) of rAAV5-miAngE or rAAV5-miSCR. Atorvastatin dose 45 mg/kg rAAV5, recombinant adeno-associated virus serotype 5. Mean is (±SD). *p ≤ 0.05 vs. Vehicle; **p ≤ 0.01 vs. Vehicle; ***p ≤ 0.001 vs. Vehicle; #p ≤ 0.05 vs. *miSCR*; ##p ≤ 0.01 vs. *miSCR*; ###p ≤ 0.001 vs. *miSCR*; &p ≤ 0.05; &&p ≤ 0.01; &&&p ≤ 0.001; ^p ≤ 0.05; ^^p ≤ 0.01; ^^^p ≤ 0.001.

between RL and FL activities. The most potent *miAng* constructs were further tested by transfecting Huh-7 cells with 10 ng of *LucAngA* or *LucAngB* and 1, 10, 50, or 250ng of each plasmid in P24-well plates.

Analysis of endogenous ANGPTL3 mRNA knockdown

Huh-7 cells were transfected in P24-well plates with 250 ng of candidate *miAng* and *miSCR* constructs and harvested 48 h later using TRIzol Reagent (Thermo Fisher Scientific). RNA was isolated using Direct-zol RNA MiniPrep (Zymo Research) according to manufacturer's instructions. DNase treatment and cDNA synthesis were performed using Ambion TURBO DNA-free DNase Treatment (ThermoFisher Scientific) and the Maxima First Strand cDNA Synthesis Kit (Thermo Fisher Scientific) according to manufacturer's instructions. Quantitative reverse transcription polymerase chain reaction (RT-qPCR) was performed using the TaqMan ready-to-use primer-probe (Thermo Fisher Scientific) from Gene Expression Assay (Thermo Fisher Scientific): ANGPTL3 (Assay ID: Hs00205581_m1, Thermo Fisher Scientific) and human β-actin (*Actb*) (housekeeping gene) (Assay ID: Hs01060665_g1, Thermo Fisher Scientific). Relative gene expression was determined by normalizing *ANGPTL3* mRNA levels against the reference gene. Results are expressed relative to the *miSCR* sample that is set to 100%.

Analysis of mature miAng

Huh-7 cells were transfected in P24-well plates with and without 250 ng or 400 ng of each candidate miAng construct, and total RNA was isolated from cells 48 h post-transfection as previously described. Small RNAs were sequenced by BaseClear B.V. and GenomeScan B.V., and endogenous mature miRNAs were annotated and quantified using the miRBase database that contains sequences of all published human miRNAs.

Analysis of miRNA expression and processing

miRNA expression and processing in transfected Huh-7 cells was performed using CLC Genomics Workbench 10. The obtained reads were adaptor-trimmed using custom adapter sequences (TGGAAT TCTCGGGTGCCAAGG for the plus strand; CCTTGGCACCC GAGAATTCCA for the minus strand). A second trimming was performed, and four nucleotides were removed from the 5′ and 3′ of each read. All reads containing ambiguity N symbols and reads <15 nucleotides or >70 nucleotides in length were excluded. The resulting unique small RNA reads were annotated using data from the miRBase database and aligned to reference sequences for the pri-*miAng* constructs. The percentage of expression for each candidate *miAng* construct in the total pool of endogenous miRNAs was calculated using CLC Genomics Workbench 10 software during the annotation process. To investigate *miAng* processing, the length and percentage of each mature miRNA species were assessed by considering the top 20 most abundant annotations (set to 100%) against the appropriate pri-*miAng* sequence.

rAAV5-miRNA production and purification

rAAV5 harboring the expression cassettes was produced by infecting expressSF+ insect cells (Protein Sciences Corporation, a Sanofi company) with two Baculoviruses, one encoding Rep and Cap and the other encoding the transgene. rAAV was purified on a fast protein liquid chromatography system (AKTA Pure, Cytiva) using AVB Sepharose (Cytiva), and titers were determined using qPCR.

In vivo studies

Mice

Female WT C57Bl/6JR mice were supplied by Janvier Labs, housed three per cage (relative humidity 40%–70%, temperature 19–24°C, and light cycle 7 AM to 6 PM), and were allowed free access to a Teklad 2916 diet. Female APOE*3-Leiden.CETP transgenic mice (TNO/InnoSer) were housed three to five mice per cage (relative humidity 40%–70%, temperature 20–24°C, light cycle 7 AM to 7 PM) and were fed a WTD (0.15% cholesterol; 15% saturated fat) with sterilized tap water ad libitum. Female mice were used because they are more responsive to dietary cholesterol and fat than males, and have higher rates of VLDL production resulting in elevated plasma TC and TG levels and an increased risk of atherosclerosis.[62] The study in WT C57Bl/6JR mice was approved by the central governmental committee on animal experiments and the animal welfare body of uniQure for the specific work protocol, in compliance with European Community specifications regarding the use of laboratory animals. The study in female APOE*3-Leiden.CETP transgenic mice was approved by the central governmental committee on animal experiments and the animal welfare body of The Netherlands Organization for Applied Scientific Research in compliance with European Community specifications regarding the use of laboratory animals.

Procedures in WT mice

Female WT C57BL/6 mice aged 7–8 weeks were injected with low, moderate, or high doses (1×10^{13}, 5×10^{13}, and 2.5×10^{14} gc/kg, respectively) of rAAV5-*miAngE* (n = 6 per group). Negative control groups included six mice injected with high-dose (2.5×10^{14} gc/kg) rAAV5-*miSCR* and six injected with vehicle control. ANGPTL3 protein levels were measured in plasma samples taken after a 4-h fast at weeks 2, 4, 6, and 8 post i.v. injection. ALT and AST activities were measured in plasma at weeks 0 (pre-treatment), 2, 4, and 8 post i.v. injection. Livers were collected after animals were euthanized at week 8, levels of *ANGPTL3* in the plasma and *miAngE* mRNA expression in livers were measured, and rAAV5 VCNs were determined.

Procedures in dyslipidemic mice

A total of 100 female APOE*3Leiden.CETP transgenic mice aged 7–13 weeks were fed a WTD during the study containing 0.15% cholesterol and 15% fat. After a 3-week run-in period, 20 low-responder mice were excluded based on TC and TG levels, and the remaining mice were divided into five groups, matched for age, body weight, and plasma TC and TG levels. Group 1 (n = 20) received vehicle control, groups 2 and 4 (n = 15 per group) received rAAV5-*miSCR*, and groups 3 and 5 (n = 15 per group) received rAAV5-*miAngE* at a moderate-high dose (1×10^{14} gc/kg). All treatments were administered at week 0 via i.v. injection into the tail vein. Blood samples were obtained 30 min after injection, and groups 4 and 5 received atorvastatin as admix to the WTD for the remainder of the study. The initial dose of atorvastatin (3.5 mg/kg diet) was increased to 4.5 mg/kg diet after week 4 to achieve a 25%–35% decrease in plasma TC levels in group 4 vs. one or both control groups (groups 1 and 2). Plasma lipid analyses were conducted in 14 mice from group 1 and in 9 per group for groups 2–5. Plasma TC and TG were measured after a 4-h fast at weeks 2, 4, 6, 8, 10, 12, 14, and 16. Lipoprotein profiles were assessed at weeks 0, 4, 8, and 12 using pooled samples per group and at week 16 using samples per mouse. The remaining six mice per group were used for toxicological profiling (plasma ALT, AST, total protein, urea, creatinine, glucose, TC, TG, and phospholipids) using fasting blood samples collected at weeks 4, 8, 12, and 16. Body weight and food intake per cage were determined at weeks 0, 1, 2, 4, 6, 8, 10, 12, 14, and 16. Five animals from group 1 were killed in week 12 and used to monitor the development of atherosclerosis in the aortic root up to that time (data not shown). The remaining animals were killed at week 16, after which plasma was obtained via heart puncture, and heart, aorta, liver, kidney, adrenal, spleen, pancreas, lung, ovarian, and brain tissue were collected. Atherosclerosis measurements were performed in the aortic root section of all mice as described below.

VCN determination in WT and dyslipidemic mice

DNA was extracted from mouse livers using the DNeasy Blood and Tissue kit (Qiagen) according to the supplier's protocol. VCNs were quantified using a TaqMan qPCR assay (Thermo Fisher Scientific) with mouse ACTB SYBR Green assay (Thermo Fisher Scientific) as a loading control gene (Forward primer: GAC ACT GGC ACA GCC AAC TTT; Reverse primer: GTG TCT ACA CCG CGG GAA TG; Probe: CTA GCG TGT AGA CTC T). Assays were performed on an ABI 7500 device (Thermo Fisher Scientific).

Angptl3 mRNA expression in WT and dyslipidemic mice

RNA was extracted from livers using the Direct-zol RNA MiniPrep (Zymo Research) according to the supplier's protocol. TURBO

DNA-free DNase Treatment (Thermo Fisher Scientific) was used to remove DNA contamination from the RNA samples. Total RNA was reverse transcribed into cDNA using the Maxima First Strand cDNA Synthesis Kit (Thermo Fisher Scientific), and qPCR was performed using the TaqMan ready-to-use primer-probe from Gene Expression Assay (Thermo Fisher Scientific): Angptl3 (Assay ID: Mm00803820_m1). mRNA expression levels were normalized to mouse *Actb* (Assay ID: Mm01205647_g1) as an internal control, and the level of gene expression was calculated relative to *miSCR*-injected mice.

Liver miAngE measurements in WT and dyslipidemic mice

RNA was extracted from mouse livers as previously described and reverse transcribed using the TaqMan MicroRNA Reverse Transcription kit (Thermo Fisher Scientific) and a custom stem-loop primer specific for *miAngE* 23 nucleotide (variant T). Custom TaqMan qPCR small RNA assays in combination with TaqMan Fast Universal kit (Thermo Fischer Scientific) were used to measure the most abundant *miAng-E* species (variant T) (Thermo Fischer Scientific, Assay ID CTGZFJPSEQ). A serial dilution of the synthetic RNA (Integrated DNA Technologies) was used to calculate the number of miAngE molecules/reaction in each liver sample. The number of molecules per cell was calculated by dividing the molecules per reaction by the cells per sample (cells per sample = pg RNA input per sample divided by 15 pg total RNA per cell).

Liver gene expression profiling in dyslipidemic mice

To investigate the potential off-target effects of rAAV5-*miAngE*, gene expression profiles were analyzed in the liver tissue of dyslipidemic APOE*3Leiden.CETP transgenic mice aged 7–11 weeks. Animals (n = 5 per group) were injected with one of the following vector constructs 5×10^{13} gc/kg of rAAV5-*mi*AngE, rAAV5-*mi*AngE scrambled control or vehicle alone (n = 5); and liver tissue was harvested 16 weeks later. Off-target analysis was performed at Fios Genomics Ltd (Edinburgh, UK). Data were generated using RNA sequencing, and reads from all samples were mapped against the mouse genome. Functional enrichment analysis was performed using the significantly differentially expressed genes identified for each condition. Both the GO[63] and Reactome[64] databases were interrogated to identify terms or pathways which were significantly enriched.

ANGPTL3 protein measurements in WT and dyslipidemic mice in plasma and liver tissue lysates

Levels of murine plasma ANGPTL3 protein and liver tissue lysates were determined using an enzyme-linked immunosorbent assay (ELISA) kit (Sigma-Aldrich, RAB0756) according to the manufacturer's instructions. Liver tissues were homogenized and processed with RIPA containing protease inhibitors to produce lysates. Plasma samples and liver tissue lysates were diluted to obtain an optical density value within the reference standard curve (generated according to the supplier's protocol), and each sample was measured in duplicate.

Lipid/lipoprotein analyses in dyslipidemic mice

Plasma TC and TG were measured from individual samples using Cholesterol CHOD-PAP and Triglycerides GPO-PAP kits (Roche/Hitachi) according to the supplier's protocol. Lipoprotein cholesterol profiles from pooled samples were determined by FLPC using an ÄKTA apparatus (GE Healthcare), and cholesterol and TG were measured in the collected fractions using the above indicated methods.

Atherosclerosis profiling in dyslipidemic mice

Formalin-fixed aortic roots were paraffin-embedded in a routine fashion, and 5-μm-thick sections were cut and mounted on 3-aminopropyltriethoxysilane-coated glass slides. After dewaxing in xylene and an ethanol gradient, slides were stained with hematoxylin, 0.25% (w/v) phloxine, and counterstained with 0.25% (w/v) saffron in ethanol. Digital microscopy images of four serial cross-sections were collected at 50-μm intervals using an Olympus BX51 microscope (Olympus). Morphometric analysis of lesion area was performed using cell^D software v2.7 (Olympus Soft Imaging Solutions), and lesion severity was scored in a blinded fashion according to the classification by the American Heart Association.[34,36,39,65]

Safety assessments in WT mice

All animals were inspected by visual monitoring once daily for signs of general discomfort or malaise and at week −1 and fortnightly from week 2 for changes in body weight per mouse, determined using a calibrated balance. ALT and AST plasma levels were determined using two commercially available kits (Sigma-Aldrich, MAK052 and MAK055) according to the manufacturer's instructions.

Safety assessments in dyslipidemic mice

All animals were inspected by visual monitoring once daily for signs of general discomfort or malaise and once weekly for changes in fur, skin, eyes, nose and mouth, posture, and explorative behavior. Body weight per mouse and food intake per cage were determined using a calibrated balance. Toxicological profiling (plasma ALT, AST, total protein, urea, creatinine, glucose, TC, TG, and phospholipids from fasting blood samples) and histopathology (heart apex, liver, spleen, pancreas, brain, kidney, lung, ovaries, and adrenal gland tissues collected after animals were euthanized) were performed by Charles River Laboratories.

Statistical analyses

Statistical analysis was performed on the ANGPTL3 protein data from WT mice using GraphPad Prism 8 using one-way ANOVA followed by the Bonferroni post-test. The Shapiro-Wilk test was used to test data from each column for normality (the recommended D'Agostino-Pearson omnibus test could not be used due to sample size n < 8). Data were not normally distributed, and the non-parametric analysis (Kruskal-Wallis test with Dunn's post-test) was applied to test the difference between population means. Statistical analyses of data from dyslipidemic mice were performed using IBM SPSS statistics 25.0. The Kolmogorov-Smirnov and Shapiro-Wilk tests were used to test for normal distribution of the data (assumed when both tests have a p value >0.05). If both tests were passed by a single time point per variable, normality was assumed for the entire variable; when more time points per variable passed both tests, normality was not assumed for the entire variable. For non-parametric calculations,

a Kruskal-Wallis test for several independent samples was used, followed by a Mann-Whitney *U*-test for independent samples. For parametric calculations, a one-way ANOVA for multiple comparisons was used, followed by Bonferroni's post hoc test. A p value ≤ 0.05 was considered statistically significant. A p value between 0.05 and 0.1 was considered as a trend toward an effect. The statistical significance threshold used to define DEGs was a false discovery rate adjustment of $p < 0.05$ and a cutoff of fold change ≥ 2 in expression. Enrichment of GO terms or Reactome pathways was statistically significant at $p < 0.05$.

DATA AVAILABILITY STATEMENT

Materials and reagents commercially procured will be shared on request. Reagents such as the AAV vectors generated by authors will not be shared unless a memorandum of understanding is signed between the research sponsoring institution and the requester. Methods are available to disclose and all data associated with this study are present within the manuscript.

SUPPLEMENTAL INFORMATION

Supplemental information can be found online at https://doi.org/10.1016/j.omtn.2023.04.004.

ACKNOWLEDGMENTS

This study was funded by uniQure biopharma B.V., Amsterdam, The Netherlands. We thank Sander van Deventer and Pavlina Konstantinova for their scientific contributions, John Kastelein for his work as SME, Martin de Haan and Maroeska Oudshoorn-Dickmann for their help with experiments, Mark van Veen for helping to generate rAAV constructs, and Raygene Martier for helping with bioinformatic analyses. Bioinformatics support was provided by Fios Genomics Ltd (Edinburgh, UK) as a commercial service. The authors thank Jackie Read, PhD, and Julia Jenkins, PhD, of GK Pharmacomm Ltd. for providing medical writing support/editorial support, which was funded by uniQure biopharma B.V. in accordance with Good Publication Practice (GPP3) guidelines (http://www.ismpp.org/gpp3).

AUTHOR CONTRIBUTIONS

V.Z.A., Y.P.L., A.V., J.M.P.L., H.M.G.P., and G.S. conceived and designed the experiments. Experiments were performed by L.P., C.V.T., H.W., T.V.Z., K.V.R., E.J.P., and N.K., and data were analyzed by V.Z.A., Y.P.L., and G.S. M.G., T.G., and E.E. contributed to the preparation of reagents, materials, and analytical tools. All authors provided critical revisions of the manuscript, provided final approval prior to submission, and agreed to be accountable for the work.

DECLARATION OF INTERESTS

V.Z. and Y.P.L. are uniQure employees, hold uniQure stocks, and are inventors on the corresponding patent application. A.V., J.M.P.L., L.P., C.V.T., H.W., T.V.Z., K.V.R., M.G., T.G., and E.E. are uniQure employees and hold uniQure stocks. E.J.P., N.K., H.M.G.P., and G.S. are employees of TNO and were employees of TNO during the time this work was conducted.

REFERENCES

1. Fire, A., Xu, S., Montgomery, M.K., Kostas, S.A., Driver, S.E., and Mello, C.C. (1998). Potent and specific genetic interference by double-stranded RNA in Caenorhabditis elegans. Nature *391*, 806–811.
2. Meister, G., and Tuschl, T. (2004). Mechanisms of gene silencing by double-stranded RNA. Nature *431*, 343–349.
3. Krek, A., Grün, D., Poy, M.N., Wolf, R., Rosenberg, L., Epstein, E.J., MacMenamin, P., da Piedade, I., Gunsalus, K.C., Stoffel, M., and Rajewsky, N. (2005). Combinatorial microRNA target predictions. Nat. Genet. *37*, 495–500.
4. Boudreau, R.L., and Davidson, B.L. (2012). Generation of hairpin-based RNAi vectors for biological and therapeutic application. Methods Enzymol. *507*, 275–296.
5. Borel, F., Kay, M.A., and Mueller, C. (2014). Recombinant AAV as a platform for translating the therapeutic potential of RNA interference. Mol. Ther. *22*, 692–701.
6. Xie, J., Mao, Q., Tai, P.W.L., He, R., Ai, J., Su, Q., Zhu, Y., Ma, H., Li, J., Gong, S., et al. (2017). Short DNA hairpins compromise recombinant adeno-associated virus genome homogeneity. Mol. Ther. *25*, 1363–1374.
7. Maestro, S., Weber, N.D., Zabaleta, N., Aldabe, R., and Gonzalez-Aseguinolaza, G. (2021). Novel vectors and approaches for gene therapy in liver diseases. JHEP Rep. *3*, 100300.
8. Liu, Y.P., Haasnoot, J., ter Brake, O., Berkhout, B., and Konstantinova, P. (2008). Inhibition of HIV-1 by multiple siRNAs expressed from a single microRNA polycistron. Nucleic Acids Res. *36*, 2811–2824.
9. Poller, W., Dimmeler, S., Heymans, S., Zeller, T., Haas, J., Karakas, M., Leistner, D.-M., Jakob, P., Nakagawa, S., Blankenberg, S., et al. (2018). Non-coding RNAs in cardiovascular diseases: diagnostic and therapeutic perspectives. Eur. Heart J. *39*, 2704–2716.
10. Osório, L., Gijsbers, R., Oliveras-Salvá, M., Michiels, A., Debyser, Z., Van den Haute, C., and Baekelandt, V. (2014). Viral vectors expressing a single microRNA-based short-hairpin RNA result in potent gene silencing in vitro and in vivo. J. Biotechnol. *169*, 71–81.
11. Xie, J., Tai, P.W.L., Brown, A., Gong, S., Zhu, S., Wang, Y., Li, C., Colpan, C., Su, Q., He, R., et al. (2020). Effective and accurate gene silencing by a recombinant AAV-compatible MicroRNA scaffold. Mol. Ther. *28*, 422–430.
12. Miniarikova, J., Zanella, I., Huseinovic, A., van der Zon, T., Hanemaaijer, E., Martier, R., Koornneef, A., Southwell, A.L., Hayden, M.R., van Deventer, S.J., et al. (2016). Design, characterization, and lead selection of therapeutic miRNAs targeting huntingtin for development of gene therapy for Huntington's disease. Mol. Ther. Nucleic Acids *5*, e297.
13. Kaadt, E., Alsing, S., Cecchi, C.R., Damgaard, C.K., Corydon, T.J., and Aagaard, L. (2019). Efficient knockdown and lack of passenger strand activity by dicer-independent shRNAs expressed from pol II-driven MicroRNA scaffolds. Mol. Ther. Nucleic Acids *14*, 318–328.
14. Cheloufi, S., Dos Santos, C.O., Chong, M.M.W., and Hannon, G.J. (2010). A dicer-independent miRNA biogenesis pathway that requires Ago catalysis. Nature *465*, 584–589.
15. Yang, J.-S., Maurin, T., Robine, N., Rasmussen, K.D., Jeffrey, K.L., Chandwani, R., Papapetrou, E.P., Sadelain, M., O'Carroll, D., and Lai, E.C. (2010). Conserved vertebrate mir-451 provides a platform for Dicer-independent, Ago2-mediated microRNA biogenesis. Proc. Natl. Acad. Sci. USA *107*, 15163–15168.
16. Keskin, S., Brouwers, C.C., Sogorb-Gonzalez, M., Martier, R., Depla, J.A., Vallès, A., van Deventer, S.J., Konstantinova, P., and Evers, M.M. (2019). AAV5-miHTT lowers huntingtin mRNA and protein without off-target effects in patient-derived neuronal cultures and astrocytes. Mol. Ther. Methods Clin. Dev. *15*, 275–284.
17. Søkilde, R., Newie, I., Persson, H., Borg, Å., and Rovira, C. (2015). Passenger strand loading in overexpression experiments using microRNA mimics. RNA Biol. *12*, 787–791.
18. Grimm, D., Streetz, K.L., Jopling, C.L., Storm, T.A., Pandey, K., Davis, C.R., Marion, P., Salazar, F., and Kay, M.A. (2006). Fatality in mice due to oversaturation of cellular microRNA/short hairpin RNA pathways. Nature *441*, 537–541.
19. Bish, L.T., Sleeper, M.M., Reynolds, C., Gazzara, J., Withnall, E., Singletary, G.E., Buchlis, G., Hui, D., High, K.A., Gao, G., et al. (2011). Cardiac gene transfer of short

hairpin RNA directed against phospholamban effectively knocks down gene expression but causes cellular toxicity in canines. Hum. Gene Ther. *22*, 969–977.

20. Borel, F., van Logtenstein, R., Koornneef, A., Maczuga, P., Ritsema, T., Petry, H., van Deventer, S.J., Jansen, P.L., and Konstantinova, P. (2011). In vivo knock-down of multidrug resistance transporters ABCC1 and ABCC2 by AAV-delivered shRNAs and by artificial miRNAs. J. RNAi Gene Silencing *7*, 434–442.

21. Spronck, E.A., Brouwers, C.C., Vallès, A., de Haan, M., Petry, H., van Deventer, S.J., Konstantinova, P., and Evers, M.M. (2019). AAV5-miHTT gene therapy demonstrates sustained huntingtin lowering and functional improvement in huntington disease mouse models. Mol. Ther. Methods Clin. Dev. *13*, 334–343.

22. Evers, M.M., Miniarikova, J., Juhas, S., Vallès, A., Bohuslavova, B., Juhasova, J., Skalnikova, H.K., Vodicka, P., Valekova, I., Brouwers, C., et al. (2018). AAV5-miHTT gene therapy demonstrates broad distribution and strong human mutant huntingtin lowering in a Huntington's disease minipig model. Mol. Ther. *26*, 2163–2177.

23. Vallès, A., Evers, M.M., Stam, A., Sogorb-Gonzalez, M., Brouwers, C., Vendrell-Tornero, C., Acar-Broekmans, S., Paerels, L., Klima, J., Bohuslavova, B., et al. (2021). Widespread and sustained target engagement in Huntington's disease minipigs upon intrastriatal microRNA-based gene therapy. Sci. Transl. Med. *13*, eabb8920.

24. Miniarikova, J., Zimmer, V., Martier, R., Brouwers, C.C., Pythoud, C., Richetin, K., Rey, M., Lubelski, J., Evers, M.M., van Deventer, S.J., et al. (2017). AAV5-miHTT gene therapy demonstrates suppression of mutant huntingtin aggregation and neuronal dysfunction in a rat model of Huntington's disease. Gene Ther. *24*, 630–639.

25. Valles, A., Brouwers, C., Pintauro, R., Snapper, J., Bohuslavova, B., Sogorb-Gonzalez, M., Fodale, V., Bresciani, A., Ellederova, Z., Blits, B., et al. (2018). I05 Sustained mutant huntingtin lowering in the brain and cerebrospinal fluid of huntington disease minipigs mediated by AAV5-MIHTT gene therapy. J. Neurol. Neurosurg. Psychiatry *89* (*Supplement 1*).

26. Reilmann, R., Ross, C., Testa, C., Frank, S., Evers, M., Haan, M., de Valles-Sanchez, A., Konstantinova, P., Deventer, S. van, and Higgins, J. (2020). Translation of AMT-130 preclinical data to inform the design of the first FDA-approved human AAV gene therapy clinical trial in adults with early manifest Huntington's disease (4531). Neurology *94*, 4531.

27. Von Drygalski, A., Giermasz, A., Castaman, G., Key, N.S., Lattimore, S., Leebeek, F.W.G., Miesbach, W., Recht, M., Long, A., Gut, R., et al. (2019). Etranacogene dezaparvovec (AMT-061 phase 2b): normal/near normal FIX activity and bleed cessation in hemophilia B. Blood Adv. *3*, 3241–3247.

28. Gomez, E., Giermasz, A., Castaman, G., Key, N., Lattimore, S., Leebeek, F., Miesbach, W., Recht, M., Von Drygalski, A., Sawyer, E., et al. (2021). Etranacogene dezaparvovec (AAV5-Padua hFIX variant, AMT-061), an enhanced vector for gene transfer in adults with severe or moderate-severe hemophilia B: 2.5 Year data from a phase 2b trial. Res Pract Thromb Haemost *5*.

29. Pipe, S.W., Leebeek, F.W., Recht, M., Key, N.S., Lattimore, S., Castaman, G., Coppens, M., Cooper, D., Gut, R., Slawka, S., et al. (2022). Adults with severe or moderately severe hemophilia B receiving etranacogene dezaparvovec in the HOPE-B phase 3 clinical trial continue to experience a stable increase in mean factor IX activity levels and durable hemostatic protection after 24 Months' follow-up. Blood *140*, 4910–4912.

30. Miesbach, W., Meijer, K., Coppens, M., Kampmann, P., Schutgens, R., Castaman, G., Sawyer, E., and Leebeek, F. (2021). Five year data confirms stable FIX expression and sustained reductions in bleeding and factor IX use following AMT-060 gene therapy in adults with severe or moderate-severe hemophilia B. Res Pract Thromb Haemost *5*.

31. Miesbach, W., Meijer, K., Coppens, M., Kampmann, P., Klamroth, R., Schutgens, R., Tangelder, M., Castaman, G., Schwäble, J., Bonig, H., et al. (2018). Gene therapy with adeno-associated virus vector 5–human factor IX in adults with hemophilia B. Blood *131*, 1022–1031.

32. Pasi, K.J., Rangarajan, S., Mitchell, N., Lester, W., Symington, E., Madan, B., Laffan, M., Russell, C.B., Li, M., Pierce, G.F., and Wong, W.Y. (2020). Multiyear follow-up of AAV5-hFVIII-SQ gene therapy for hemophilia A. N. Engl. J. Med. *382*, 29–40.

33. Chen, P.-Y., Gao, W.-Y., Liou, J.-W., Lin, C.-Y., Wu, M.-J., and Yen, J.-H. (2021). Angiopoietin-like protein 3 (ANGPTL3) modulates lipoprotein metabolism and dyslipidemia. Int. J. Mol. Sci. *22*, 7310.

34. Dewey, F.E., Gusarova, V., Dunbar, R.L., O'Dushlaine, C., Schurmann, C., Gottesman, O., McCarthy, S., Van Hout, C.V., Bruse, S., Dansky, H.M., et al. (2017). Genetic and pharmacologic inactivation of ANGPTL3 and cardiovascular disease. N. Engl. J. Med. *377*, 211–221.

35. Reeskamp, L.F., Millar, J.S., Wu, L., Jansen, H., van Harskamp, D., Schierbeek, H., Gipe, D.A., Rader, D.J., Dallinga-Thie, G.M., Hovingh, G.K., and Cuchel, M. (2021). ANGPTL3 inhibition with evinacumab results in faster clearance of IDL and LDL apoB in patients with homozygous familial hypercholesterolemia-brief report. Arterioscler. Thromb. Vasc. Biol. *41*, 1753–1759.

36. Pouwer, M.G., Heinonen, S.E., Behrendt, M., Andréasson, A.C., van Koppen, A., Menke, A.L., Pieterman, E.J., van den Hoek, A.M., Jukema, J.W., Leighton, B., et al. (2019). The APOE*3-Leiden heterozygous glucokinase knockout mouse as novel translational disease model for type 2 diabetes, dyslipidemia, and diabetic atherosclerosis. J. Diabetes Res. *2019*, 9727952.

37. Kühnast, S., Fiocco, M., van der Hoorn, J.W.A., Princen, H.M.G., and Jukema, J.W. (2015). Innovative pharmaceutical interventions in cardiovascular disease: focusing on the contribution of non-HDL-C/LDL-C-lowering versus HDL-C-raising: a systematic review and meta-analysis of relevant preclinical studies and clinical trials. Eur. J. Pharmacol. *763*, 48–63.

38. Zadelaar, S., Kleemann, R., Verschuren, L., de Vries-Van der Weij, J., van der Hoorn, J., Princen, H.M., and Kooistra, T. (2007). Mouse models for atherosclerosis and pharmaceutical modifiers. Arterioscler. Thromb. Vasc. Biol. *27*, 1706–1721.

39. Groot, P.H., van Vlijmen, B.J., Benson, G.M., Hofker, M.H., Schiffelers, R., Vidgeon-Hart, M., and Havekes, L.M. (1996). Quantitative assessment of aortic atherosclerosis in APOE*3 Leiden transgenic mice and its relationship to serum cholesterol exposure. Arterioscler. Thromb. Vasc. Biol. *16*, 926–933.

40. Setten, R.L., Rossi, J.J., and Han, S.-P. (2019). The current state and future directions of RNAi-based therapeutics. Nat. Rev. Drug Discov. *18*, 421–446.

41. Traber, G.M., and Yu, A.-M. (2023). RNAi-based therapeutics and novel RNA bioengineering Technologies. J. Pharmacol. Exp. Therapeut. *384*, 133–154.

42. Ruotsalainen, A.-K., Mäkinen, P., and Ylä-Herttuala, S. (2021). Novel RNAi-based therapies for atherosclerosis. Curr. Atherosclerosis Rep. *23*, 45.

43. Bofill-De Ros, X., and Gu, S. (2016). Guidelines for the optimal design of miRNA-based shRNAs. Methods *103*, 157–166.

44. Zheng, B., Mai, Q., Jiang, J., and Zhou, Q. (2019). The therapeutic potential of small activating RNAs for colorectal carcinoma. Curr. Gene Ther. *19*, 140–146.

45. Kühnast, S., van der Hoorn, J.W.A., Pieterman, E.J., van den Hoek, A.M., Sasiela, W.J., Gusarova, V., Peyman, A., Schäfer, H.L., Schwahn, U., Jukema, J.W., and Princen, H.M.G. (2014). Alirocumab inhibits atherosclerosis, improves the plaque morphology, and enhances the effects of a statin. J. Lipid Res. *55*, 2103–2112.

46. van den Hoek, A.M., van der Hoorn, J.W.A., Maas, A.C., van den Hoogen, R.M., van Nieuwkoop, A., Droog, S., Offerman, E.H., Pieterman, E.J., Havekes, L.M., and Princen, H.M.G. (2014). APOE*3Leiden.CETP transgenic mice as model for pharmaceutical treatment of the metabolic syndrome. Diabetes Obes. Metabol. *16*, 537–544.

47. High, K.A. (2014). Gene therapy for hemophilia: the clot thickens. Hum. Gene Ther. *25*, 915–922.

48. High, K.A., George, L.A., Eyster, M.E., Sullivan, S.K., Ragni, M.V., Croteau, S.E., Samelson-Jones, B.J., Evans, M., Joseney-Antoine, M., Macdougall, A., et al. (2018). A phase 1/2 trial of investigational spk-8011 in hemophilia a demonstrates durable expression and prevention of bleeds. Blood *132*, 487.

49. Mingozzi, F., Anguela, X.M., Pavani, G., Chen, Y., Davidson, R.J., Hui, D.J., Yazicioglu, M., Elkouby, L., Hinderer, C.J., Faella, A., et al. (2013). Overcoming pre-existing humoral immunity to AAV using capsid decoys. Sci. Transl. Med. *5*, 194ra92.

50. Rangarajan, S., Walsh, L., Lester, W., Perry, D., Madan, B., Laffan, M., Yu, H., Vettermann, C., Pierce, G.F., Wong, W.Y., and Pasi, K.J. (2017). AAV5-Factor VIII gene transfer in severe hemophilia. N. Engl. J. Med. *377*, 2519–2530.

51. Pipe, S., Leebeek, F.W.G., Ferreira, V., Sawyer, E.K., and Pasi, J. (2019). Clinical considerations for capsid choice in the development of liver-targeted AAV-based gene transfer. Mol. Ther. Methods Clin. Dev. *15*, 170–178.

52. Adam, R.C., Mintah, I.J., Alexa-Braun, C.A., Shihanian, L.M., Lee, J.S., Banerjee, P., Hamon, S.C., Kim, H.I., Cohen, J.C., Hobbs, H.H., et al. (2020). Angiopoietin-like protein 3 governs LDL-cholesterol levels through endothelial lipase-dependent VLDL clearance. J. Lipid Res. *61*, 1271–1286.

53. Musunuru, K., Pirruccello, J.P., Do, R., Peloso, G.M., Guiducci, C., Sougnez, C., Garimella, K.V., Fisher, S., Abreu, J., Barry, A.J., et al. (2010). Exome sequencing, ANGPTL3 mutations, and familial combined hypolipidemia. N. Engl. J. Med. *363*, 2220–2227.

54. Grundy, S.M., Stone, N.J., Bailey, A.L., Beam, C., Birtcher, K.K., Blumenthal, R.S., Braun, L.T., de Ferranti, S., Faiella-Tommasino, J., Forman, D.E., et al. (2019). 2018 AHA/ACC/AACVPR/AAPA/ABC/ACPM/ADA/AGS/APhA/ASPC/NLA/PCNA guideline on the management of blood cholesterol: a report of the american college of cardiology/american heart association task force on clinical practice guidelines. J. Am. Coll. Cardiol. *73*, e285–e350.

55. Mach, F., Baigent, C., Catapano, A.L., Koskinas, K.C., Casula, M., Badimon, L., Chapman, M.J., De Backer, G.G., Delgado, V., Ference, B.A., et al. (2020). 2019 ESC/EAS Guidelines for the management of dyslipidaemias: lipid modification to reduce cardiovascular risk. Eur. Heart J. *41*, 111–188.

56. Satny, M., Hubacek, J.A., and Vrablik, M. (2021). Statins and inflammation. Curr. Atherosclerosis Rep. *23*, 80.

57. Wang, J., Zheng, W., Zheng, S., Yuan, Y., Wen, W., Cui, W., Xue, L., Sun, X., Shang, H., Zhang, H., et al. (2023). Targeting ANGPTL3 by GalNAc-conjugated siRNA ANGsiR10 lowers blood lipids with long-lasting and potent efficacy in mice and monkeys. Mol. Ther. Nucleic Acids *31*, 68–77.

58. Nathwani, A.C., Reiss, U.M., Tuddenham, E.G.D., Rosales, C., Chowdary, P., McIntosh, J., Della Peruta, M., Lheriteau, E., Patel, N., Raj, D., et al. (2014). Long-term safety and efficacy of factor IX gene therapy in hemophilia B. N. Engl. J. Med. *371*, 1994–2004.

59. Manno, C.S., Pierce, G.F., Arruda, V.R., Glader, B., Ragni, M., Rasko, J.J., Ozelo, M.C., Hoots, K., Blatt, P., Konkle, B., et al. (2006). Successful transduction of liver in hemophilia by AAV-Factor IX and limitations imposed by the host immune response. Nat. Med. *12*, 342–347.

60. Vroon, D.H., and Israili, Z. (1990). Aminotransferases. In Clinical Methods: The History, Physical, and Laboratory Examinations, 3rd Edition, H.K. Walker, W.D. Hall, and J.W. Hurst, eds. (Boston: Butterworths).

61. Zuker, M. (2003). Mfold web server for nucleic acid folding and hybridization prediction. Nucleic Acids Res *31*, 3406–3415.

62. van Vlijmen, B.J., van 't Hof, H.B., Mol, M.J., van der Boom, H., van der Zee, A., Frants, R.R., Hofker, M.H., and Havekes, L.M. (1996). Modulation of very low density lipoprotein production and clearance contributes to age- and gender- dependent hyperlipoproteinemia in apolipoprotein E3-Leiden transgenic mice. J. Clin. Invest. *97*, 1184–1192.

63. Ashburner, M., Ball, C.A., Blake, J.A., Botstein, D., Butler, H., Cherry, J.M., Davis, A.P., Dolinski, K., Dwight, S.S., Eppig, J.T., et al. (2000). Gene ontology: tool for the unification of biology. The Gene Ontology Consortium. Nat. Genet. *25*, 25–29.

64. Gillespie, M., Jassal, B., Stephan, R., Milacic, M., Rothfels, K., Senff-Ribeiro, A., Griss, J., Sevilla, C., Matthews, L., Gong, C., et al. (2022). The reactome pathway knowledgebase 2022. Nucleic Acids Res. *50*, D687–D692.

65. Stary, H.C., Chandler, A.B., Dinsmore, R.E., Fuster, V., Glagov, S., Insull, W., Rosenfeld, M.E., Schwartz, C.J., Wagner, W.D., and Wissler, R.W. (1995). A definition of advanced types of atherosclerotic lesions and a histological classification of atherosclerosis. A report from the Committee on Vascular Lesions of the Council on Arteriosclerosis, American Heart Association. Arterioscler. Thromb. Vasc. Biol. *15*, 1512–1531.